Capacitive aptasensor based on interdigitated electrode for breast cancer detection in undiluted human serum

Sunil K. Arya[1*], Pavel Zhurauski[1], Pawan Jolly[1], Marina R. Batistuti[2], Marcelo Mulato[2], Pedro Estrela[1*]

[1]Department of Electronic & Electrical Engineering, University of Bath, Bath BA2 7AY, United Kingdom

[2]Department of Physics, University of São Paulo, 14040-901, Ribeirão Preto, SP, Brazil

[*]*Corresponding Authors:* Phone: +44 7405106621, Email: *sunilarya333@gmail.com* (Sunil K Arya), *P.Estrela@bath.ac.uk* (Pedro Estrela)

Abstract

We report the development of a simple and powerful capacitive aptasensor for the detection and estimation of human epidermal growth factor receptor 2 (HER2), a biomarker for breast cancer, in undiluted serum. The study involves the incorporation of interdigitated gold electrodes, which were used to prepare the electrochemical platform. A thiol terminated DNA aptamer with affinity for HER2 was used to prepare the bio-recognition layer via self-assembly on interdigitated gold surfaces. Non-specific binding was prevented by blocking free spaces on surface via starting block phosphate buffer saline-tween20 blocker. The sensor was characterized using cyclic voltammetry, electrochemical impedance spectroscopy (EIS), atomic force microscopy and contact angle studies. Non-Faradic EIS measurements were utilized to investigate the sensor performance via monitoring of the changes in capacitance. The

aptasensor exhibited logarithmically detection of HER2 from 1 pM to 100 nM in both buffer and undiluted serum with limits of detection lower than 1 pM. The results pave the way to develop other aptamer-based biosensors for protein biomarkers detection in undiluted serum.

Keywords: Aptamer; impedimetric; capacitance; biosensor; HER2; breast cancer

1. Introduction

Breast cancer is one of the most common cancers and the second major cause of deaths in women worldwide (Diaconu et al. 2013; Siegel et al. 2013). More than 90% of these deaths are related to metastatic growth (Siegel et al. 2013). Therefore, early stage detection of cancer is crucial to increase the chances of survival. Human epidermal growth factor receptors (HER/erbB) are involved in normal growth and cell differentiation, however a malignant growth can be related with overexpression of human epidermal growth factor receptor 2 (HER2), a transmembrane tyrosine kinase receptor expressed and involved in the growth of certain cancer cells. It is present in some cases of breast, ovarian, lung, gastric, oral, prostate and other cancers (Patris et al. 2014). HER2 has also been shown to be overexpressed in around 20–30% of aggressive breast cancers and associated with poor prognosis (Diaconu et al. 2013). Breast cancer patients possess high HER2 concentrations in their blood (14–75 ng/ml) compared to normal individuals (4–14 ng/ml) and can be utilized for diagnosis and active surveillance of patients at risk or in treatment (Chun et al. 2013; Hung et al. 1995). To evaluate these concentrations, various HER2 detection techniques have been reported, including fluorescence in situ hybridization (FISH) assays and immunohistochemical (IHC) assays (Press et al. 2002). However, these techniques require sophisticated instrumentation, special training, are labour-intensive and time-consuming.

To satisfy the unmet clinical need of point-of-care biomarker detection, several biosensors that use enzymes, receptors and antibodies have been reported (Camacho et al. 2009; Wang et al. 2009b). One of the disadvantages of using antibodies is their instability due to irreversible denaturation. Therefore, alternative bio-recognition elements are desirable to develop stable biosensors. Synthetic molecules such as oligonucleotide aptamers have shown great promise to fulfil these gaps associated with biomarkers. Aptamers, single strand oligonucleotides (DNA or RNA) that are designed and developed synthetically in the

laboratory, have been shown to bind to specific targets such as proteins (Qureshi et al. 2015). Aptamers are known to be more stable, cheaper, are easily modified chemically and can be easily produced in bulk. Furthermore, the unique binding properties of aptamers have shown great potential for biosensors using optical, electrochemical, and mass-sensitive approaches (Cho et al. 2009; Qureshi et al. 2015).

Among various types of biosensors, electrochemical techniques have gained much interest due to their simplicity, miniaturizability, faster and more sensitive response (Arya and Bhansali 2012; Bollella et al. 2017; Wang et al. 2017). For electrochemical biosensor preparation, self-assembled monolayers (SAM), magnetic beads and nanomaterials such as graphene and nanocomposites have gained considerable attention (Arya et al. 2009; Filip et al. 2015; Hammond et al. 2016; Kurlyandskaya and Miyar 2007; Lan et al. 2017; Selwyna et al. 2013). Although nanomaterial-based sensors can be fabricated with high sensitivity due to e.g. high surface-to-volume ratios, the use of SAMs on microelectrodes has the advantage of simple single-step biomolecular surface chemistries with high reproducibility and low cost. Among electrochemical biosensors, electrochemical impedance spectroscopy (EIS)-based biosensors are recently gaining much attention (Barsoukov and Macdonald 2005; Gong et al. 2017; Guan et al. 2004; Katz and Willner 2003). EIS based biosensors allow the label-free detection of an analyte binding to a bio-recognition layer at the electrode surface and can be measured in the form of changes in capacitance and/or resistance (Ramón-Azcón et al. 2008). It has been shown in the literature that the use of interdigitated microelectrodes (IDμEs) to develop EIS-based biosensors present additional advantages of faster reaction kinetics, enhanced sensitivity and improved signal-to-noise ratio (Arya and Bhansali 2012; Ramón-Azcón et al. 2008; Wang et al. 2009a). Moreover, due to faster mass transport with a lower *iR* drop and double layer charging effects, IDμEs attain steady state faster, resulting in easier measurement than with conventional macroelectrodes (Arya and Bhansali 2012; Varshney and Li 2009).

Impedimetric biosensors can be operated in both Faradaic and non-Faradaic modes. In Faradaic impedance, a redox couple is required, which is interchangeably oxidized and reduced via electron transfer to and from the electrode surface (Daniels and Pourmand 2007); transduction happens via changes in the hindrance presented by the surface interface to a redox-containing solution phase (Arya et al. 2014; Santos et al. 2014). On the other hand, in a non-Faradaic measurement charging currents are dominant and capacitive changes occurring via changes in the hindrance presented by the surface dielectric, charge distribution or local conductance are monitored (Berggren et al. 2001; Luo and Davis 2013). Non-Faradaic approaches have the advantage of not requiring the pre-addition of redox probes to the analytical solution and can be applied for highly sensitive detection of analytes in a more amenable manner for point-of-care applications (Berggren et al. 2001; Daniels and Pourmand 2007; Qureshi et al. 2010). Furthermore, for practical applications, where the measurement in real samples is required, non-Faradaic measurements are desirable. Non-Faradaic electrochemical impedance spectroscopy (EIS) has also been used to characterize the interfacial properties of biomaterials or cells associated with conductive or semiconductive devices, where the measured signals are attributed to the insulating effects of biomaterials or membranes of cells that grow on or attach to the sensing surface (Lin et al. 2015). Such capacitance change may arise when a target protein binds to the receptor immobilized onto electrode surface, displacing water molecules and ions away from the surface (Tkac and Davis 2009), or due to varying protein conformation (Berggren et al. 2001).

In this study, the combination of interdigitated micro electrodes (IDμE), DNA aptamers and capacitive measurements has been utilized to develop a simple and sensitive biosensor for HER2 protein biomarker estimation. HER2 can be estimated using direct measurement of the serum protein levels or by analysis of HER2 nucleic acid sequences. Direct protein measurement, as the one presented in this work, makes sample processing easier and hence

amenable for use in a point-of-care platform. For biosensor development, gold IDμE chips were functionalized with DNA aptamers via self-assembly and used for specific capture of HER2 protein. The surface was further blocked using phosphate buffer saline-tween 20 based starting block (SB) to prevent non-specific binding and fouling of the surface. The non-Faradaic electrochemical impedance spectroscopy was utilized to quantify HER2 binding events in buffer and serum samples by monitoring the changes in capacitance.

2. Experimental

2.1. Materials

Thiol terminated HER2 specific DNA aptamer (5'-SH-$(CH2)_6$-AAC CGC CCA AAT CCC TAA GAG TCT GCA CTT GTC ATT TTG TAT ATG TAT TTG GTT TTT GGC TCT CAC AGA CAC ACT ACA CAC GCA CA-3') was procured from Sigma (UK). This HER2 aptamer sequence was taken from the report of Liu et al. (2012), where the authors have developed and characterized the aptamer (HB5) by using systematic evolution of ligands by exponential enrichment technology (SELEX). The developed aptamer was an 86-nucleotide DNA molecule that bound to an epitope peptide of HER2 with a K_d of 18.9 nM. For binding studies, different concentrations of HER2 (R&D Systems, UK) and other targets were prepared in 10 mM PBS, pH 7.4 or in undiluted serum. StartingBlock phosphate buffer saline-Tween 20 (SB) was procured from Fisher Scientific (UK); Dulbecco's phosphate buffered saline (PBS) and phosphate buffered saline with 0.05% tween 20 (PBST-20) were procured from Sigma (UK). All other chemicals were of analytical grade and were used without further purification. All aqueous solutions were prepared using 18.2 MΩ cm ultra-pure water (milli-Q water) with a Pyrogard® filter (Millipore, MA, USA).

2.2. Measurement and apparatus

Blank and aptamer modified IDμE chips were characterized via atomic force microscopy (AFM) imaging in ambient tapping mode using a MultiMode NanoScope with IIIa controller (Bruker, Germany) in conjunction with version 6 control software. AFM images were recorded using 10 nm diameter AFM ContAl-G tips (BudgetSensors®, Bulgaria), and then processed by the NanoScope Analysis software, version 1.5. Aptamer binding was also characterized via contact angle measurements using an in-house built optical angle measurement system (Miodek et al. 2015). For measurement, chips were placed on a stage and a 10 µl of water drop was dispensed on the electrode with the dispensing system. The wetting of surface was then captured using a Nikon p520 camera. Contact angle was measured using a screen protractor version 4.0 procured from Iconico.

Biosensor fabrication was also characterized electrochemically in Faradaic mode via electrochemical impedance spectroscopy (EIS) and cyclic voltammetry (CV) in a three-electrode configuration with on-chip gold (2 mm wide) as counter and *pseudo* reference electrode. EIS measurements were performed at open circuit potential (equilibrium potential), without external biasing in the frequency range of 100 kHz – 100 mHz with a 25 mV amplitude using a µAutolab III / FRA2 potentiostat/galvanostat (Metrohm, Netherlands). EIS and CV measurements were carried out using 50 µl of PBS solution (10 mM, pH 7.4) containing a mixture of 5 mM $Fe(CN)_6^{4-}$ (ferrocyanide) and 5 mM of $Fe(CN)_6^{3-}$ (ferricyanide) as a redox probe couple. Non-Faradaic EIS measurements on IDμEs (in the absence of redox couple) using a two-electrode configuration were utilized for HER2 detection and estimation in 10 mM PBS (pH 7.4) in a frequency range 100 kHz – 100 mHz with a 200 mV amplitude. Each experiment has been done at least in triplicated using different sensors. Only the optimized sensors in terms of concentration of reagents providing reproducible, reliable and sensitive performance are presented here.

2.3 Electrode preparation and functionalisation

2.3.1 Gold electrode fabrication

The deposition of interdigitated gold micro-electrode arrays on silicon/silicon oxide wafers was performed using standard lithographic and micro-fabrication techniques as previously described (Pui et al. 2013). The 3200 μm long interdigitated fingers of 5 μm, spaced at 10 μm and attached to single base of 5500 μm length were deposited and utilized for biosensor development. The prepared IDμEs were cleaned thoroughly with isopropyl alcohol, acetone and with excess amounts of milli-Q water followed by 30 min UV-ozone treatment (ProCleaner, BioForce Nanosciences, USA) before aptamer functionalization.

2.3.2 Aptamer assembly and blocking

For thiolated aptamer assembly and immobilization on IDμEs, stock aptamer immobilisation solution (100 μM in tris buffer) was heated to 95°C for 5 min followed by ice cooling to room temperature and thereafter, diluted to 2 μM solution in PBS 1x pH 7.4. Pre-cleaned IDμEs were then incubated with 2 μM aptamer solution for 120 min at room temperature. Later, the chips were washed with PBST-20 (pH 7.4) and PBS (10 mM. pH 7.4) to remove any unbound aptamers. The free spaces on the chip were blocked using SB incubation for 30 min, after which extra solution was removed and the developed sensor electrodes were stored at 4^{o}C till further use. Figure 1 shows the schematic for aptasensor electrode preparation. During the electrode preparation, the thiolated aptamer forms a self-assembled monolayer (SAM) on the old surface of chip via interactions between the alkane chains on the 5'. The SB blocker fills the free spaces between aptamer molecules on the chip and prevents the non-specific adsorption of serum proteins on the surface during incubation. Furthermore, the two middle IDμEs provide the opportunity to use a two-electrode system for non-Faradaic measurement of HER2 without any redox couple.

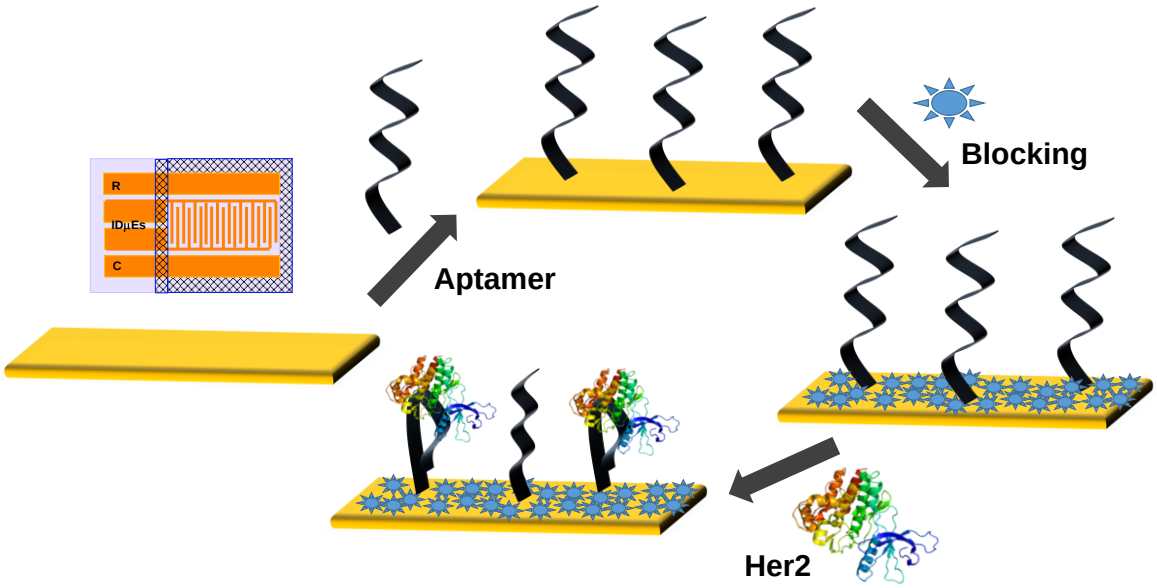

Figure 1. Schematic for aptasensor electrode preparation

3. Results and Discussion

3.1. Characterisation of the biosensor fabrication

3.1.1 *Contact angle and AFM measurements*

Figures 2a and 2b show the variation of contact angle of blank gold and after aptamer immobilization. The clear decrease in contact angle value from 23º for blank gold to 10º for the aptamer/IDμE suggests the successful formation of an aptamer self-assembled monolayer (SAM). Furthermore, Figures 2c and 2d show the AFM images of blank gold and aptamer modified surface taken in tapping mode using a 10 nm AFM tip. The observed change in non-uniform morphology for blank gold (Figure 2c) surface to uniformly distributed structure (Figure 2d) for aptamer modified IDμE confirms the successful SAM formation by thiolated aptamer. The mean roughness (R_a) and maximum roughness (R_{max}) change from 1.46 nm and 11.8 nm for blank to 1.36 and 9.53 nm for the aptamer modified surface, respectively, indicating surface functionalization. These changes could be attributed to aptamer binding making the surface smoother.

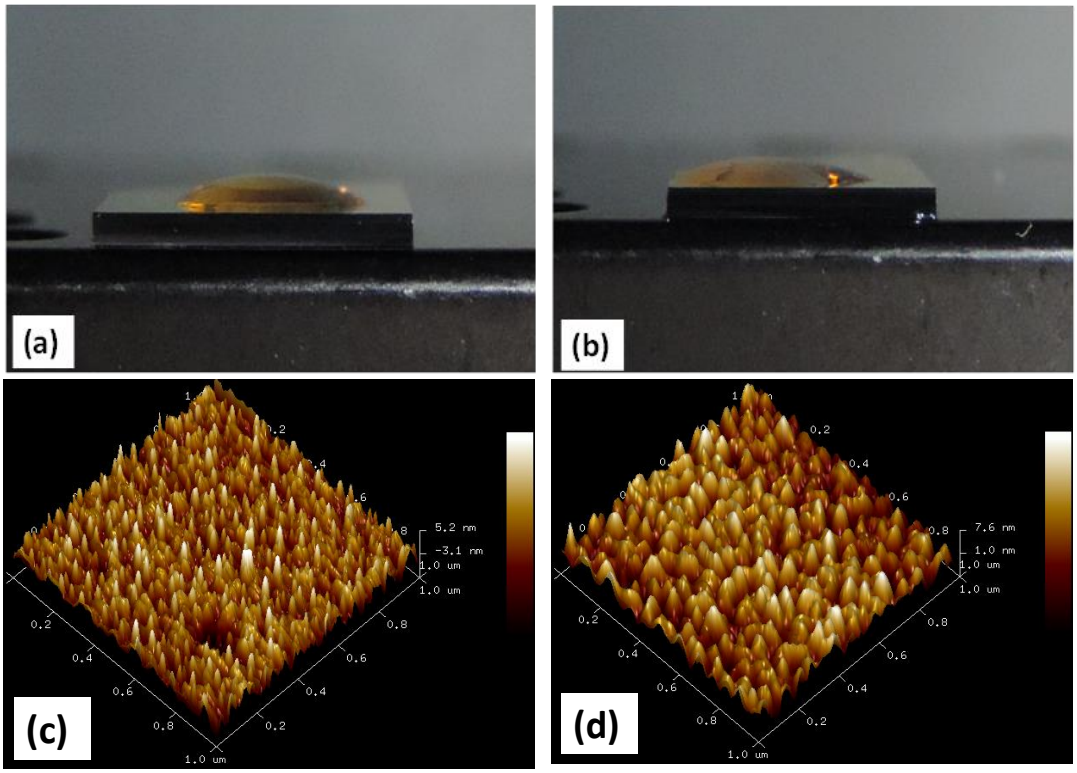

Figure 2. Contact angle image for (a) blank cleaned gold surface, (b) after aptamer SAM formation and AFM image for (c) blank cleaned gold surface, (d) after aptamer SAM formation

3.2 CV and EIS characterization for biosensor development

In order to further confirm the aptamer immobilization, the sensor was characterized using cyclic voltammetry (CV) in PBS (1x) containing 5 mM potassium ferrocynide and 5 mM potassium ferricynide, $[Fe(CN)_6]^{3-/4-}$. Figure 3a shows a decrease in peak current from 156 µA for blank IDµE to 132 µA for aptamer SAM, indicating successful SAM formation. Furthermore, the reduction in peak current to 96 µA after blocking confirms the filling of free surface on IDµEs with blocker proteins. Figure 3b shows the Nyquist plots for each step, with an increase in charge transfer resistance (R_{ct}) from 217 Ω for blank chip to 661 Ω after aptamer SAM formation, again revealing successful immobilization. The increase in R_{ct} to 1021 Ω after

blocking can be attributed to adsorption of non-conducting blocker proteins in free areas of the gold electrodes.

Blank, aptamer modified and after blocking electrodes were further investigated under different scan rates (30 – 100 mV/s), and oxidation and reduction peaks were observed even after aptamer SAM formation and blocking, suggesting good redox activity of the electrodes. Moreover, the observed linear variation in oxidation peak currents with square root of scan rate (Figures 3c) obeying equations 1 to 3, suggests a diffusion controlled process on sensor surface (Vasudev et al. 2013). For repeated sets, the error was found to be less than 2% for blank chips, increasing to around 4% for fabricated chips after aptamer binding and blocking with SB.

$$I_{oxi}\ (Blank\ ID\mu E)\ (\mu A) = -21.62\ \mu A + 796.85\ (Scan\ rate)^{1/2}\ \mu A;\ r^2 = 0.999 \quad (1)$$

$$I_{oxi}\ (Aptamer/ID\mu E)\ (\mu A) = 18.99\ \mu A + 504.33\ (Scan\ rate)^{1/2}\ \mu A;\ r^2 = 0.999 \quad (2)$$

$$I_{oxi}\ (SB\text{-}Aptamer/ID\mu E)\ (\mu A) = 20.69\ \mu A + 340.81\ (Scan\ rate)^{1/2}\ \mu A;\ r^2 = 0.991 \quad (3)$$

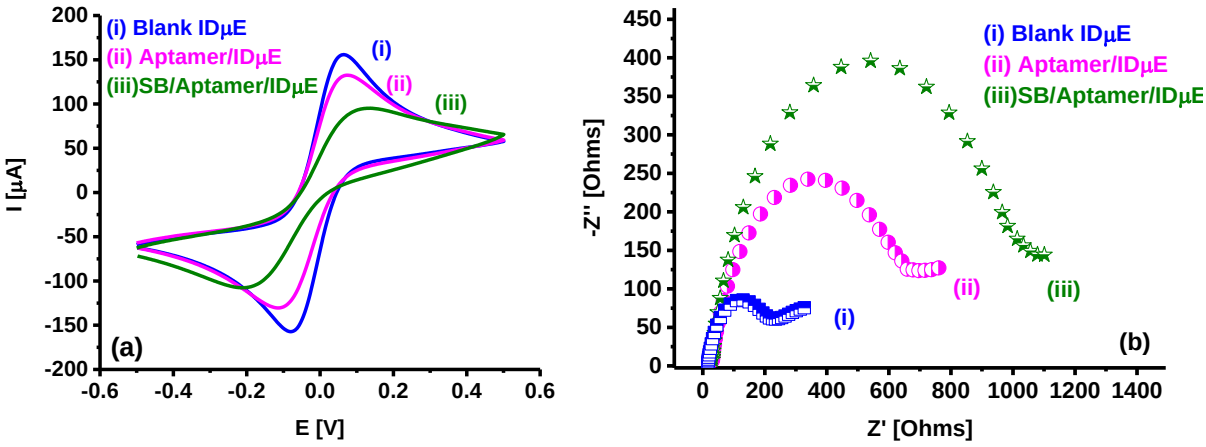

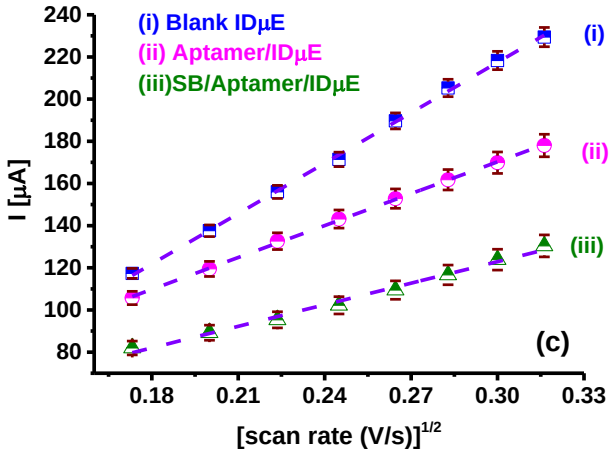

Figure 3. Characterization of biosensor electrode fabrication at each step via (a) CV, (b) EIS and (c) scan rates study showing oxidation peak current response as a function of square root of scan rate.

3.2 HER2 studies

3.2.1 Capacitive measurement via electrochemical impedance for HER2 in PBS

The SB-Aptamer/IDμE bio-electrodes were utilized to study aptamer-HER2 binding on surface in the 1 pM to 100 nM concentration range (Figure 4). For the measurements, 50 µl of the desired HER2 concentrations were placed in contact with the bio-electrode and incubated for 30 min, followed by washing with PBST20 and PBS to remove unbound HER2 molecules. The non-Faradic EIS spectra was then recorded in 10 mM PBS (pH 7.4) and then 1/ωZ" (ω is the angular frequency and Z" the imaginary part of the impedance) was utilized to estimate the capacitance of the system. A maximum in the phase angle (Figure 4a) was observed at 2 Hz, indicating maximum a capacitive effect at this frequency. Capacitive values at 2 Hz (Figure 4b) were then utilized to plot the calibration curve for HER2 concentrations in PBS (Figure 4c). The decreasing capacitance values observed for increasing HER2 concentrations is attributed to the successful capture of HER2 proteins onto the surface bound aptamer. This change in capacitance in non-Faradaic measurement can be attributed to the insulating effects of HER2

proteins that attach to the sensing surface and displacing water molecules/ions away from the surface (Tkac and Davis 2009), or due to varying aptamer/protein conformation (Berggren et al. 2001). The calibration plot generated using relative change in capacitance (Figure 4c) shows that the bio-electrode can be used for linear detection of HER2 on logarithmic scale in the 1 pM to 100 nM range and can be characterized using ΔC (µF) = 0.049 (µF) + 0.071 log [HER2] (pM). Furthermore, the bio-electrode exhibited a sensitivity of 0.071 µF/ log([HER2] pM) and a correlation coefficient of 0.982. Different electrodes were found to exhibit similar responses within 5% as shown by the error bars in Figure 4c.

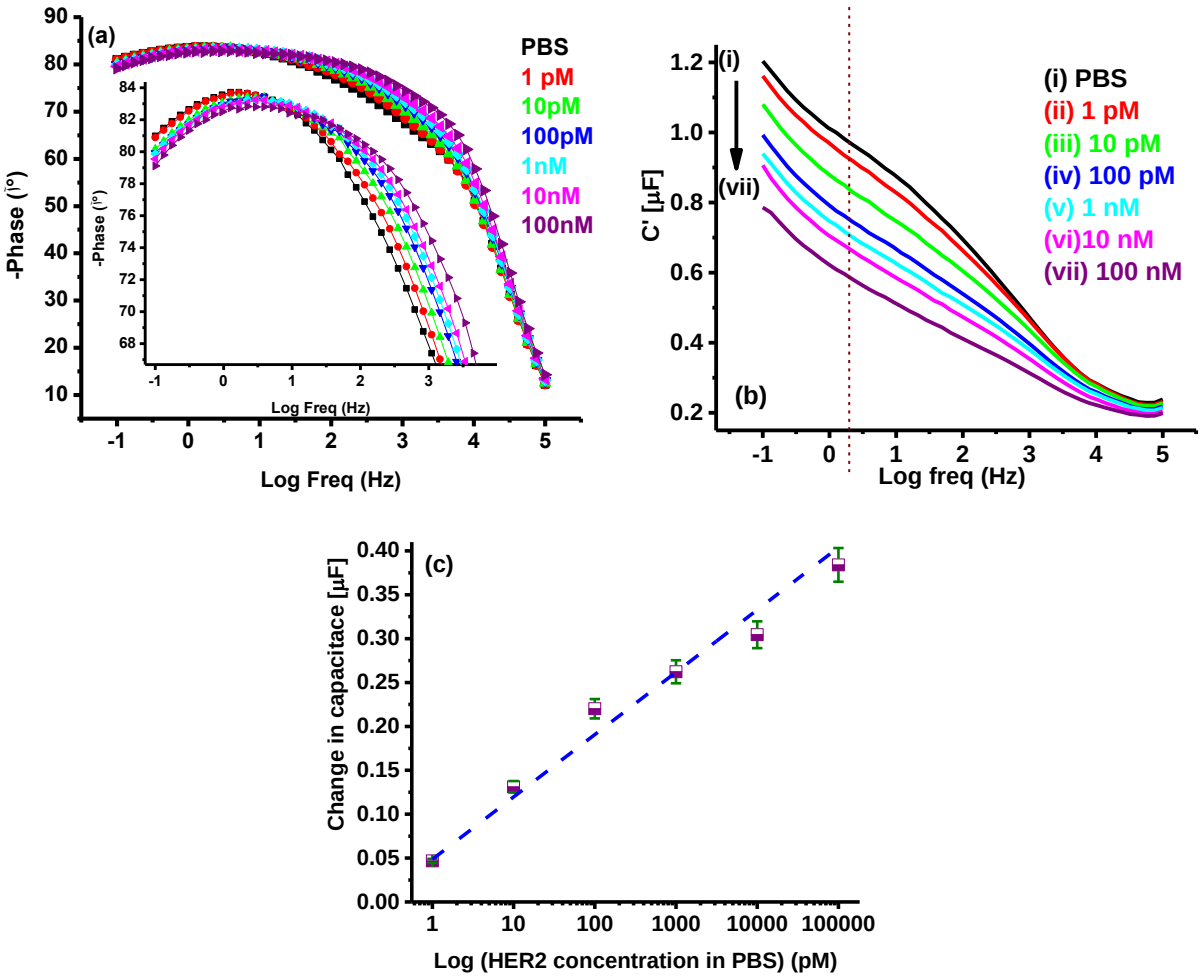

Figure 4. (a) Phase data, (b) capacitance data for aptamer-HER2 binding on biosensor surface in PBS and (c) calibration curve using capacitance data for different concentration at 2 Hz

3.2.2 Capacitive measurement via electrochemical impedance for HER2 in undiluted serum

In order to test the applicability of the sensors for clinical applications, SB-Aptamer/IDμE bio-electrodes were tested with undiluted serum spiked with HER2. This enabled to study the effect of all types of serum proteins on the interaction between surface bound aptamer and HER2 molecules in the concentration range 1 pM to 100 nM (Figure 5). Similarly to HER2 in PBS, the bioassay and non-Faradaic EIS measurements were carried out for HER2 in serum and the capacitance calculated for different HER2 concentrations (Figure 5b). Capacitance values at 1 Hz, where the maximum phase angle is observed (Figure 5a), were used for the calibration curve in Figure 5c. The observed maximum in phase angle at slightly lower frequency may be attributed to the presence of serum proteins and different conductivity and ionic strength of HER2 in the serum samples as compared to the HER2 samples in PBS. The plots in Figure 5b, showing a decrease in capacitance for increasing HER2 concentrations in serum, clearly indicate that the bio-electrode can be successfully utilized for HER2 estimation in serum. The calibration plot in Figure 5c indicates that the bio-electrodes can be used for detection of HER2 in the range 1 pM to 100 nM at 1 Hz and can be characterized using ΔC (μF) = 0.057 (μF) + 0.035 log [HER2] (pM). Furthermore, the bio-electrode exhibited a sensitivity of 0.035 μF/ log([HER2] pM) with a correlation coefficient of 0.98. Different electrodes were found to exhibit similar responses within 5%, as shown by the error bars in Figure 5c. The observed lower sensitivity of 0.035 μF/ log([HER2] pM) for HER2 detection in serum in comparison to 0.071 μF/ log([HER2] pM) in PBS might be attributed to the presence of serum proteins in the sample causing hindrance in aptamer-HER2 interaction. Repeated experiments showed similar and consistent responses, indicating that the lower sensitivity in serum samples will not affect the accurate estimation of HER2. Furthermore, other than serum proteins, the bio-electrodes were also tested for specificity against proteins such as PSA (at a high concentration of 100 ng/ml), thrombin (100 ng/ml) and HER4 (100 ng/ml) spiked in serum (data not shown) and found to exhibit negligible signal when compared with signal for the

serum only samples, indicating good selectivity of the developed electrode. Furthermore, other than serum proteins, the bio-electrodes were also tested for specificity against proteins such as PSA (at a high concentration of 100 ng/ml), thrombin (100 ng/ml) and HER4 (100 ng/ml) spiked in serum (Figure 5d). From Fig 5d, it is clear that bio-electrode is specific and exhibits negligible signals for interferents when compared with the signal for the serum only samples.

The data obtained in this work was compared to other sensors reported in the literature for HER2 estimation (Table 1). The present system exhibits better response than those previously reported and can be utilized for real sample applications. It should be noted that Qureshi et al. (2015) obtained a similar LOD with interdigitated electrodes but their work was carried out at high frequencies (50–350 MHz), which are difficult to implement in a low cost point-of-care system; also the dynamic range in that work is considerably smaller (0.2–2 ng/ml), requires longer incubation times (2h) and 10 times dilution of serum.

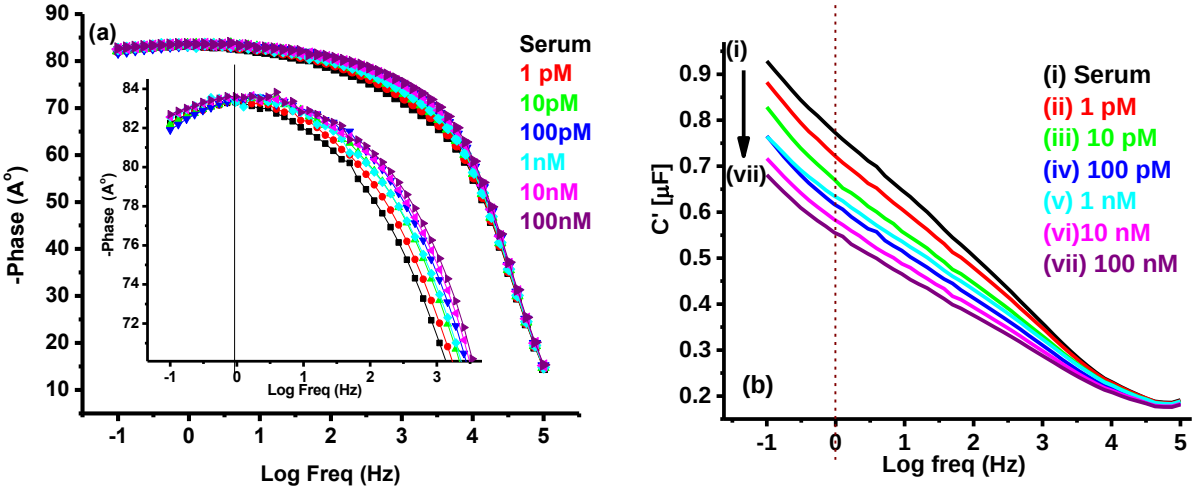

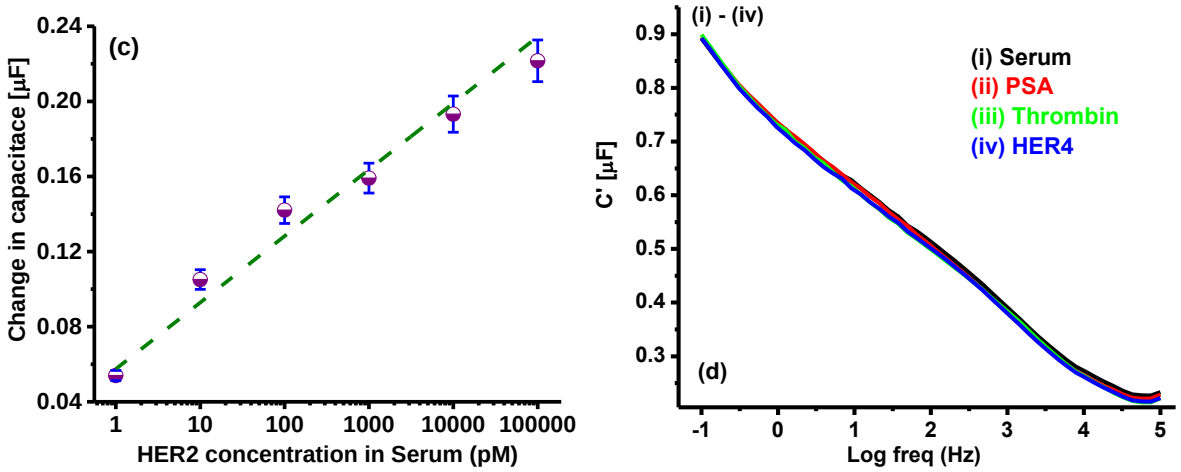

Figure 5. (a) Phase data, (b) capacitance data for interaction between surface bound aptamer with HER2 concentrations in undiluted serum, (c) calibration curve using capacitance data for different concentration at 1 Hz, (d) capacitance data for interference study.

Table 1: Comparison between the present approach and state-of-art technologies

Technique	**Electrode/Surface**	**Probe**	**LOD**	**Reference**
Fluorescence	Carbon nanotube wrapped anti-HER2 ssDNA aptamers	Aptamer	4750 ng/ml (38 nM)	(Niazi et al. 2015)
Microfluidic with fluorescence transduction	Quantum Dots (QD)	Immunoassay / Antibody	0.27 ng/ml	(Jokerst et al. 2009)
Opto-fluidic ring resonator (OFRR)	Silica glass capillaries modified with cross-linkers to bind protein G	Antibody	10 ng/ml	(Gohring et al. 2010)
Surface plasmon resonance (SPR) spectroscopy	Protein G based	Antibody	11 ng/ml	(Martin et al. 2006)
Surface acoustic wave (SAW)	SAW resonator with gold transducer	Antibody	10 ng/ml	(Gruhl et al. 2010)
Surface acoustic wave (SAW)	SAW resonators based on 36° YX-Li-TaO3 substrates	Antibody	10 ng/ml	(Gruhl and Länge 2012)
Amperometric (CV)	Carbon screen printed electrodes	Nano-Immunoassay / Antibody	1000 ng/ml	(Patris et al. 2014)
EIS	Gold nanostructured screen-printed graphite	Affibody	6 ng/ml	(Ravalli et al. 2015)
Capacitance	Interdigitated microelectrodes	Aptamer	0.2 ng/ml	(Qureshi et al. 2015)
Capacitance	**Interdigitated electrodes**	**Aptamer**	**0.1 ng/ml (1 pM)**	**Present study**

4. Conclusion

An aptamer based capacitive biosensor strategy has been demonstrated for the detection of HER2 in undiluted serum. The biosensor showed excellent selectivity when challenged with other serum proteins. The prepared biosensor exhibited a wide HER2 detection dynamic range from 1 pM to 100 nM range, with a high sensitivity of 0.035 μF/ log([HER2] pM) in undiluted serum. The detection limits are lower than those previously reported in the literature for HER2 sensing, enabling better early cancer diagnosis and monitoring of cancer progression and/or treatment. Measurements can be performed at a single frequency, making instrumentation for a point-of-care device easy to implement. Furthermore, the fabrication method is simple and can be applied for the detection of other biomarkers in serum samples, paving the way to a new generation of alternative low cost and rapid biosensors.

Acknowledgements

S.K.A. was funded by a Marie Skłodowska-Curie Individual Fellowship through the European Commission's Horizon 2020 Programme (grant no. 655176). P.Z and P.J. were funded by the European Commission FP7 Programme through the Marie Curie Initial Training Network PROSENSE (grant no. 317420, 2012-2016). M.R.B. was funded by FAPESP (process number 2015/14403-5). M.M. and P.E. acknowledge funding from FAPESP and the University of Bath through the SPRINT programme.

References

Arya, S.K., Bhansali, S., 2012. Biosensors Journal 1, H110601, 11060.

Arya, S.K., Kongsuphol, P., Wong, C.C., Polla, L.J., Park, M.K., 2014. Sensors and Actuators B: Chemical 194, 127-133.

Arya, S.K., Solanki, P.R., Datta, M., Malhotra, B.D., 2009. Biosensors and Bioelectronics 24(9), 2810-2817.

Barsoukov, E., Macdonald, J.R. (Eds.), 2005. Impedance Spectroscopy: Theory, Experiment, and Applications. John Wiley & Sons; 2005.

Berggren, C., Bjarnason, B., Johansson, G., 2001. Electroanalysis 13(3), 173-180.

Bollella, P., Fusco, G., Tortolini, C., Sanzò, G., Favero, G., Gorton, L., Antiochia, R., 2017. Biosensors and Bioelectronics 89, Part 1, 152-166.

Camacho, C., Chico, B., Cao, R., Matías, J.C., Hernández, J., Palchetti, I., Simpson, B.K., Mascini, M., Villalonga, R., 2009. Biosensors and Bioelectronics 24(7), 2028-2033.

Cho, E.J., Lee, J.-W., Ellington, A.D., 2009. Annual Review of Analytical Chemistry 2(1), 241-264.

Chun, L., Kim, S.-E., Cho, M., Choe, W.-s., Nam, J., Lee, D.W., Lee, Y., 2013. Sensors and Actuators B: Chemical 186, 446-450.

Daniels, J.S., Pourmand, N., 2007. Electroanalysis 19(12), 1239-1257.

Diaconu, I., Cristea, C., Hârceagă, V., Marrazza, G., Berindan-Neagoe, I., Săndulescu, R., 2013. Clinica Chimica Acta 425, 128-138.

Filip, J., Kasák, P., Tkac, J., 2015. Chemical Papers 69(1), 112-133.

Gohring, J.T., Dale, P.S., Fan, X., 2010. Sensors and Actuators B: Chemical 146(1), 226-230.

Gong, Q., Wang, Y., Yang, H., 2017. Biosensors and Bioelectronics 89, Part 1, 565-569.

Gruhl, F.J., Länge, K., 2012. Analytical Biochemistry 420(2), 188-190.

Gruhl, F.J., Rapp, M., Länge, K., 2010. Procedia Engineering 5, 914-917.

Guan, J.-G., Miao, Y.-Q., Zhang, Q.-J., 2004. Journal of Bioscience and Bioengineering 97(4), 219-226.

Hammond, J.L., Formisano, N., Estrela, P., Carrara, S., Tkac, J., 2016. Essays in Biochemistry 60(1), 69-80.

Hung, M.-C., Matin, A., Zhang, Y., Xing, X., Sorgi, F., Huang, L., Yu, D., 1995. Gene 159(1), 65-71.

Jokerst, J.V., Raamanathan, A., Christodoulides, N., Floriano, P.N., Pollard, A.A., Simmons, G.W., Wong, J., Gage, C., Furmaga, W.B., Redding, S.W., McDevitt, J.T., 2009. Biosensors and Bioelectronics 24(12), 3622-3629.

Katz, E., Willner, I., 2003. Electroanalysis 15(11), 913-947.

Kurlyandskaya, G.V., Miyar, V.F., 2007. Biosensors and Bioelectronics 22(9-10) 2341-2345.

Lan, L., Yao, Y., Ping, J., Ying, Y., 2017. Biosensors and Bioelectronics 91(Supplement C), 504-514.

Lin, S.-P., Vinzons, L.U., Kang, Y.-S., Lai, T.-Y., 2015. ACS Applied Materials & Interfaces 7(18), 9866-9878.

Liu, Z., Duan, J.-H., Song, Y.-M., Ma, J., Wang, F.-D., Lu, X., Yang, X.-D., 2012. Journal of Translational Medicine 10(1), 148..

Luo, X., Davis, J.J., 2013. Chemical Society Reviews 42(13), 5944-5962.

Martin, V.S., Sullivan, B.A., Walker, K., Hawk, H., Sullivan, B.P., Noe, L.J., 2006. Applied Spectroscopy 60(9), 994-1003.

Miodek, A., Regan, E., Bhalla, N., Hopkins, N., Goodchild, S., Estrela, P., 2015. Sensors 15(10), 25015-25032.

Niazi, J.H., Verma, S.K., Niazi, S., Qureshi, A., 2015. Analyst 140(1), 243-249.

Patris, S., De Pauw, P., Vandeput, M., Huet, J., Van Antwerpen, P., Muyldermans, S., Kauffmann, J.-M., 2014. Talanta 130, 164-170.

Press, M.F., Slamon, D.J., Flom, K.J., Park, J., Zhou, J.-Y., Bernstein, L., 2002. Journal of Clinical Oncology 20(14), 3095-3105.

Pui, T.S., Kongsuphol, P., Arya, S.K., Bansal, T., 2013. Sensors and Actuators B: Chemical 181, 494-500.

Qureshi, A., Gurbuz, Y., Niazi, J.H., 2010. Procedia Engineering 5, 828-830.

Qureshi, A., Gurbuz, Y., Niazi, J.H., 2015. Sensors and Actuators B: Chemical 220, 1145-1151.

Ramón-Azcón, J., Valera, E., Rodríguez, Á., Barranco, A., Alfaro, B., Sanchez-Baeza, F., Marco, M.P., 2008. Biosensors and Bioelectronics 23(9), 1367-1373.

Ravalli, A., da Rocha, C.G., Yamanaka, H., Marrazza, G., 2015. Bioelectrochemistry 106, Part B, 268-275.

Santos, A., Davis, J.J., Bueno, P.R., 2014. J Anal Bioanal Tech, S7:016.

Selwyna, P.G.C., Loganathan, P.R., Begam, K.H., 2013. 2013 International Conference on Signal Processing , Image Processing & Pattern Recognition, pp. 75-81.

Siegel, R., Naishadham, D., Jemal, A., 2013. CA: A Cancer Journal for Clinicians 63(1), 11-30.

Tkac, J., Davis, J.J., 2009. Chapter 7 Label-free Field Effect ProteinSensing. Engineering the Bioelectronic Interface: Applications to Analyte Biosensing and Protein Detection, pp. 193-224. The Royal Society of Chemistry.

Varshney, M., Li, Y., 2009. Biosensors and Bioelectronics 24(10), 2951-2960.

Vasudev, A., Kaushik, A., Bhansali, S., 2013. Biosensors and Bioelectronics 39(1), 300-305.

Wang, L., Xiong, Q., Xiao, F., Duan, H., 2017. Biosensors and Bioelectronics 89, Part 1, 136-151.

Wang, R., Wang, Y., Lassiter, K., Li, Y., Hargis, B., Tung, S., Berghman, L., Bottje, W., 2009a. Talanta 79(2), 159-164.

Wang, X., Zhao, M., Nolte, D.D., 2009b. Analytical and Bioanalytical Chemistry 393(4), 1151–1156.